Atmos. Chem. Phys. Discuss., 13, 32229–32267, 2013
www.atmos-chem-phys-discuss.net/13/32229/2013/
doi:10.5194/acpd-13-32229-2013

Atmospheric Chemistry and Physics Discussions

Sensitivity analysis of an updated bidirectional air-surface exchange model for mercury vapor

X. Wang[1,2], **C.-J. Lin**[1,3,4], **and X. Feng**[1]

[1]State Key Laboratory of Environmental Geochemistry, Institute of Geochemistry, Chinese Academy of Sciences, Guiyang, China
[2]University of Chinese Academy of Sciences, Beijing, China
[3]Department of Civil Engineering, Lamar University, Beaumont, TX, USA
[4]College of Environment and Energy, South China University of Technology, Guangzhou, China

Received: 13 June 2013 – Accepted: 22 November 2013 – Published: 10 December 2013

Correspondence to: C.-J. Lin (jerry.lin@lamar.edu) and X. Feng (fengxinbin@vip.skleg.cn)

Published by Copernicus Publications on behalf of the European Geosciences Union.

Abstract

A box model for estimating bidirectional air-surface exchange of gaseous elemental mercury (Hg^0) has been updated based on the latest understanding of the resistance scheme of atmosphere–biosphere interface transfer. Simulations were performed for two seasonal months to evaluate diurnal and seasonal variation. The base-case results show that water and soil surfaces are net sources while vegetation is a net sink of Hg^0. The estimated net exchange in a domain covering the contiguous US and part of Canada and Mexico is 38 and 56 Mg as evasion in the summer and winter month. The smaller evasion in summer is due to stronger Hg^0 uptake by vegetation. Modeling experiments using a 2-level factorial design were conducted to examine the sensitivity of flux response to changes of physical and environmental parameters in the model. It is shown that atmospheric shear flow (surface wind over water and friction velocity over terrestrial surfaces), dissolved gaseous mercury (DGM) concentration, soil organic and Hg content, and air temperature are the most influential factors. The positive effect of friction velocity and soil Hg content on the evasion flux from soil and canopy can be effectively offset by the negative effect of soil organic content. Significant synergistic effects are identified between surface wind and DGM level for water surface, and between soil Hg content and friction velocity for soil surface, leading to ~ 50 % enhanced flux compared to the sum of their individual effects. The air-foliar exchange is mainly controlled by surface resistance terms controlled by solar irradiation and air temperature. Research in providing geospatial distribution of Hg in water and soil will greatly improve the flux estimate. Elucidation on the kinetics and mechanism of Hg(II) reduction in soil/water and quantification of the surface resistances specific to Hg species will also help reduce the model uncertainty.

ACPD

13, 32229–32267, 2013

1 Introduction

Mercury (Hg) is a persistent, bioaccumulative pollutant released into the atmosphere from a variety of anthropogenic and natural sources. The anthropogenic release ($2000 \sim 2400\,\mathrm{Mg\,yr^{-1}}$) primarily comes from fossil fuel combustion, waste incineration, metal smelting and cement production (Pacyna et al., 2003, 2006; Pirrone et al., 2010; Streets et al., 2005, 2009). The natural sources include geological weathering from Hg enriched substrates, biomass burning, volcanic activities and other Hg^0 exchange, including so-called re-emission, at the atmosphere–biosphere interface (Gustin et al., 2008; Mason and Sheu, 2002). While the men-made emissions were estimated and continuously updated with reasonable consistency since the 1990s, the estimates for natural emissions have been highly uncertain ($1500–5207\,\mathrm{Mg\,yr^{-1}}$), primarily due to a lack of understanding in the air-surface exchange of Hg^0. Since the natural release can account for up to two-thirds of global mercury input to the atmosphere (Friedli et al., 2009; Pirrone et al., 2010), better quantification of the mass input is critical in assessing the global biogeochemical cycling of mercury (Lindberg et al., 2007).

Air–surface exchange model is an important component in atmospheric mercury models for estimating Hg^0 evasion and deposition over soil, water and vegetation. For terrestrial surfaces, the evasion from soil has been calculated using the statistical relationships obtained from the measured Hg^0 flux and observed environmental factors such as temperature, solar irradiance and Hg content (Bash et al., 2004; Gbor et al., 2006; Lin et al., 2005; Shetty et al., 2008; Xu et al., 1999). Such an approach oversimplifies the role of environmental factors in the exchange process because Hg^0 flux was measured only in a limited number of locations where the environmental parameters (such as soil properties and meteorology) are specific to those sites. Using the limited measurement data for extrapolating the flux estimate in a large geographical area may not be representative. In addition, these models treat vegetation as a net evasion source of Hg^0, which is inconsistent with later assessments that suggest vegetation a net sink (Gustin et al., 2008; Hartman et al., 2009). More recently, algorithms

ACPD
13, 32229–32267, 2013

representing the transport resistances at soil and foliage interfaces were developed to calculate the multilayered, bidirectional flux through Hg concentration gradient between ambient level and a "compensation" point inferred from the surface characteristics (Bash, 2010; Bash et al., 2007; Scholtz et al., 2003; Zhang et al., 2009a). This approach is more scientifically sound and mathematically robust. The model results also seem to be more consistent with those measured from stable isotope studies (Bash, 2010). However, the complicated model parameterization makes it difficult to understand the relative importance of model variables on the simulated flux. It also requires assumptions for numerous model variables that lack field data to confine their values. Although the model results can be constrained by air concentration and wet deposition, the assumptions could increase the uncertainty of model estimates and limits the improvement of model algorithms.

The objectives of this study are to present an updated Hg^0 air–surface exchange model and to quantitatively examine the relative importance of the physical and environmental variables implemented in the model. Coupled with the latest understanding in the partitioning and mass transfer at different atmosphere–biosphere interfaces, we integrated the bidirectional air–surface exchange model (Bash, 2010; Bash et al., 2007) and the surface resistance schemes of Hg dry deposition (Lin et al., 2006; Zhang et al., 2003, 2009a) for quantifying the air–surface exchange of Hg^0. Two monthly simulations were performed to investigate the seasonal and diurnal variability of the model-estimated flux. A systematic set of sensitivity simulations using multi-step factorial designs of experiments were performed to investigate the effect of significant model parameters and their interplays. Based on the sensitivity results, processes that control Hg^0 air–surface exchange over different natural surfaces are discussed and research needs for future model improvement are proposed.

ACPD
13, 32229–32267, 2013

2 Methods

2.1 Model description

The total air–surface exchange is the sum of Hg^0 fluxes from water, soil (including bare lands and soil under the canopy) and foliage surfaces. The direction (evasion or deposition) of the flux is driven by the gradient between atmospheric Hg^0 concentration and a surface compensation point that represents the Hg^0 concentration at the interface between the atmosphere and a natural surface. The magnitude of the flux is determined by the ratio of concentration gradient to surface resistance (for terrestrial surfaces) or by the product of overall mass transfer coefficient and concentration gradient (for water surfaces). The nomenclature and dimension of the entire set of model variables are detailed in Table 1. The parameterization of each model component is briefly described below.

2.2 Air–water exchange

The flux over fresh water and oceanic surfaces, F_w, is calculated using a two-film mass transfer model with the transfer rate limited by the diffusion in the water boundary layer (Poissant et al., 2000):

$$F_w = K_w(C_w - \frac{C_{atm}}{H_w}) \quad (1)$$

where K_w is the overall mass transfer coefficient estimated by the wind speed at 10 m above water surface and the mass transfer ratio of CO_2/Hg across the air–water interface (Shetty et al., 2008), C_w is the DGM concentration in surface water, H_w is the dimensionless Henry's law constant. K_w and H_w are calculated using formulation described earlier (Lin and Tao, 2003; Poissant et al., 2000).

ACPD
13, 32229–32267, 2013

2.3 Air–terrestrial exchange

The terrestrial system is divided into two categories: the canopy biomes (leaf area index, LAI > 0) and the bare lands (LAI = 0, referring to barren or sparsely vegetated land, bare ground tundra and snow or ice surface). Over the canopy system, a multi-layer canopy resistance scheme modified after Bash (2010) and Zhang et al. (2003) was applied (Fig. 1). The flux over canopy biomes, F_{cnp}, is estimated as:

$$F_{cnp} = \frac{\Delta t}{(R_a + R_b)}(\chi_{cnp} - C_{atm}) \quad (2)$$

where Δt is time duration, R_a is the aerodynamic resistance, R_b is the quasi-laminar sub-layer resistance, C_{atm} is the atmospheric Hg concentration. R_a and R_b are calculated according to Marsik et al. (2007). χ_{cnp} is the overall compensation point parameterized as a weighted average of exchange coefficients at the air–cuticle, air–stomata, and air–soil interfaces as illustrated in Fig. 1 (Bash, 2010; Zhang et al., 2009a):

$$\chi_{cnp} = \frac{\frac{\chi_c}{R_c} + \frac{\chi_s}{R_s} + \frac{\chi_g}{R_g+R_{ac}} + \frac{C_{atm}}{R_a+R_b}}{\frac{1}{R_c} + \frac{1}{R_s} + \frac{1}{R_g+R_{ac}} + \frac{1}{R_a+R_b}} \quad (3)$$

where χ_c is the cuticular compensation point, χ_s is the stomatal compensation point, χ_g is the soil compensation point, R_c is the cuticular resistance, R_s is the stomatal resistance, R_g is the soil diffusion resistance, R_{ac} is the in-canopy aerodynamic resistance.

2.3.1 Air–soil exchange

In absence of vegetation (when LAI = 0), the flux from bare lands (F_{bls}) can be estimated as:

$$F_{bls} = \frac{\Delta t}{R_a + R_b + R_g}(\chi_g - C_{atm}) \quad (4)$$

ACPD
13, 32229–32267, 2013

In the presence of vegetation (when LAI > 0), the flux from soil under canopy (F_g) is calculated as:

$$F_g = \frac{\Delta t}{R_g + R_{ac}}(\chi_g - \chi_{cnp}) \quad (5)$$

The compensation point at air–soil interface (χ_g) can be expressed as (Bash, 2010):

$$\chi_g = \frac{\left[Hg^0\right]_{sl} H}{f_{oc} K_{oc}} \quad (6)$$

where $\left[Hg^0\right]_{sl}$ is the concentration of Hg^0 bound to soil, calculated as a reduction product of Hg(II) using soil Hg content and a pseudo-first-order rate constant related to solar irradiance (Gustin et al., 2002). H is Henry's constant parameterized following Andersson et al. (2008). f_{oc} is the fraction of organic carbon in surface soil (0–5 cm). K_{oc} is the partition coefficient of Hg^0 between soil organic carbon and water.

R_g is the Hg^0 diffusion resistance over a ground surface (soil, ice/snow) (Zhang et al., 2002b):

$$\frac{1}{R_g} = \frac{\alpha_{Hg^0}}{R_{g(SO_2)}} + \frac{\beta_{Hg^0}}{R_{g(O_3)}} \quad (7)$$

where $R_{g(SO_2)}$ and $R_{g(O_3)}$ are the diffusion resistances of SO_2 and O_3, α_{Hg^0} is the Hg^0 scaling factor based on SO_2, β_{Hg^0} is Hg^0 scaling factor based on O_3. The formulation of $R_{g(SO_2)}$ and $R_{g(O_3)}$ has been described previously (Zhang et al., 2003). R_{ac} accounts for the resistance of gas diffusion from ground to the lower canopy and is assumed to be common for all gaseous species (Zhang et al., 2002b).

ACPD
13, 32229–32267, 2013

2.3.2 Air–cuticle exchange

Air–cuticle exchange flux is calculated as (Bash, 2010):

$$F_c = \frac{\Delta t}{R_c}(\chi_c - \chi_{cnp}) \quad (8)$$

$$\chi_c = \frac{[Hg_c^0]}{LAP} \quad (9)$$

where LAP denotes the leaf–air partitioning coefficient for Hg^0 (Rutter et al., 2011), $[Hg_c^0]$ is the concentration of Hg^0 bound to foliar cuticular surface, calculated as the photoreduction product of a fraction of newly deposited Hg(II) on foliar interfaces (Graydon et al., 2009):

$$[Hg_c^0] = f_{rxn}[Hg_{c,DD}^{II+}] \quad (10)$$

$$\left[Hg_c^{II+}\right] = (1 - f_{rxn} - f_{fixed})[Hg_{c,DD}^{II+}] \quad (11)$$

$$\left[Hg_c^{II+}\right] = \frac{[Hg_w^{II+}]}{T_l} \quad (12)$$

where $[Hg_{c,DD}^{II+}]$ is the concentration loading of total dry deposited Hg(II) on cuticle, $\left[Hg_c^{II+}\right]$ is the concentration of the deposited Hg(II) residing on cuticular surfaces, $[Hg_w^{II+}]$ is the concentration of Hg(II) that can be washed off from leaves, f_{rxn} is the fraction of Hg(II) that can be photo-reduced, f_{fixed} is the fraction of Hg(II) fixed into tissue and not available for re-emission or wash-off, T_l is the leaf thickness. f_{rxn}, f_{fixed} are parameterized following Smith-Downey et al. (2010). R_c is the cuticular resistance calculated as (Zhang et al., 2002b):

$$\frac{1}{R_c} = \frac{\alpha_{Hg^0}}{R_{c(SO_2)}} + \frac{\beta_{Hg^0}}{R_{c(O_3)}} \quad (13)$$

ACPD
13, 32229–32267, 2013

2.3.3 Air–stomata exchange

The air–stomata exchange flux is estimated as (Bash, 2010):

$$F_s = \frac{\Delta t}{R_s}(\chi_s - \chi_{cnp}) \quad (14)$$

$$\chi_s = \frac{[Hg_s^0]}{K_{LA}} \quad (15)$$

It is assumed that the uptake of Hg species through stomata is predominantly Hg^0 due to its abundance in the atmosphere (Capiomont et al., 2000; Millhollen et al., 2006; Stamenkovic and Gustin, 2009). As such, the dissolved Hg^0 in the stomatal compartment, $[Hg_s^0]$, can be formulated as:

$$[Hg_s^0] = (1 - f_{fixed})[Hg_{s,DD}^0] \quad (16)$$

where $[Hg_{s,DD}^0]$ is the concentration of newly deposited Hg^0 stored in the stomatal compartment. The overall stomatal resistance is calculated as (Zhang et al., 2002b):

$$R_s = \frac{R_{st} + R_{me}}{1 - W_{st}} \quad (17)$$

where R_{st} is the resistance associated with stomata, R_{me} is resistance associated with mesophyll reservoir, W_{st} is the fraction of stomatal blocking under wet condition. The detailed formulation of R_{st} and R_{me} and W_{st} can be found elsewhere (Zhang et al., 2012, 2003, 2002b).

2.4 Modeling experiments for sensitivity analysis

A series of 2-level factorial designs of experiments were performed to assess the sensitivity to changes of model variables as well as their synergistic and antagonistic interactions. The studied variables include both physical and environmental parameters.

ACPD
13, 32229–32267, 2013

Their respective experimental levels are show in Tables 2–4. The principle of factor sparsity (Myers et al., 2009) states that the main effects and lower-order interactions dominate most system responses and the higher-order interaction is not significant. Therefore, the effect of interaction terms higher than second order was not considered.

For water surface, there are four factors driving the model simulation (Table 2). Therefore, a 2^4 full factorial design was applied. For bare lands, the 11 model parameters (Table 3) form a 2^{11-6} fractional design (Resolution IV) enabling main effects free from aliasing. The number of runs (32), although intensive, is still manageable. After this initial screening, a two-level full factorial design was applied for the significant factors based on a 95 % confidence level (results of the 2^{11-6} design are shown in the Supplement). For the canopy ecosystem, 15 main factors (Table 4) were selected to form a 2^{15-9} fractional design (Resolution IV, 64 experiments). In this case, the alias system is more complex because of the large number of study factors. Therefore, a successive $2^{(11-6)}$ design (Supplement) was applied to the pre-screened significant factors to obtain 5 most significant factor for a 2^5 full factorial design (Supplement). The sensitivity results were illustrated based on the final full factorial design for watersheds, bare lands, canopy ecosystems. The data analysis of the factorial experiments was conducted using Minitab 16.

2.5 Model configuration and data

The modeling domain is in Lambert Conformal projection covering mainly the Contiguous United States (CONUS), with 156 × 118 grid cells at 36 km spatial resolution. Hourly meteorological data were prepared using the Weather Research and Forecasting (WRF) model Version 3.4 with the Noah Land Surface Model. The model algorithms were coded in FORTRAN 90 and Network Common Data Form (NetCDF) version 4.1. The gridded model results were visualized by the Visualization Environmental for Rich Data Interpretation (VERDI) version 1.4.

A base-case simulation was performed in a summer and a winter month (August and December 2009) to evaluate the seasonal and diurnal variability of the air–surface

ACPD
13, 32229–32267, 2013

exchange. The base case refers to the modeling utilizing the values listed in Table 1 with the meteorological parameters extracted from WRF output. In the simulation, the atmospheric Hg^0 concentration retrieved from the output of the Hg extension of Community Multi-scale Air Quality modeling system (CMAQ-Hg) version 4.6 for the same modeling period was applied to represent the air concentration of Hg^0. The simulation does not directly incorporate the feedback of the air–surface exchange to the air concentration. However, for a regional model domain (CONUS), natural evasion and deposition of Hg^0 does not significantly modify the ambient concentration (Lin et al., 2005; Gbor et al., 2006). In the factorial model experiments, the concentration of Hg^0 was tested as a sensitivity parameter.

3 Results and discussion

3.1 Results of base-case simulations

The model estimates a net emission of 38.4 Mg in the summer month (16.6 Mg from water, 45.0 Mg from soil and −23.2 Mg from foliage) and 56.0 Mg in the winter month (33.9 Mg from water, 29.5 Mg from soil and −7.4 Mg from foliage) for the entire domain. The evasion from water body accounts for ∼ 50 % of the total natural emission because of the large water areal coverage in the domain (59 %). Vegetation represents a net sink, this is different from earlier estimates using the evapotranspiration approach (Bash et al., 2004; Shetty et al., 2008) but consistent with recent observational studies (Gustin et al., 2008; Stamenkovic and Gustin, 2009). For the terrestrial system, the total emission is 43.9 Mg in two months. Assuming the annual emission is about 5–6 times of the two monthly sum, the model-estimated annual natural emission is comparable to recent estimates in the contiguous US (95–150 $Mg\,yr^{-1}$) (Ericksen et al., 2006; Hartman et al., 2009; Zehner and Gustin, 2002).

ACPD
13, 32229–32267, 2013

3.1.1 Air–water exchange

The mean simulated flux over water surface is 1.6 and 3.1 $ng\,m^{-2}\,h^{-1}$ in the summer and winter month (Figs. 2a and 3a). Water body is a net source, producing fluxes typically in the range of 1–4 $ng\,m^{-2}\,h^{-1}$, similar to earlier measurements (Andersson et al., 2011; Mason et al., 2001a). The spatial distribution is primarily driven by the surface wind speed. Temperature, air Hg^0 and DGM concentration play a much less significant role because a constant DGM was assumed (40 $ng\,m^{-3}$) and the Hg^0 level over water was in a narrow range (1.4 ~ 1.8 $ng\,m^{-3}$). The Pearsons's correlation coefficient (r) between flux and wind speed is much stronger than the value between flux and temperature (0.56 vs. 0.18). The flux in the winter month is greater because of stronger winds in the northeastern corner of the domain. The emission flux does not show clear diurnal variation in both months because wind speed is the most dominant factor (Fig. 4a).

3.1.2 Air–soil exchange

Soil surfaces have been suggested to be a net source of Hg (Gustin et al., 2008; Hartman et al., 2009), which is also shown in the base-case model results (Figs. 2 and 3). The mean flux from bare lands (0.7 and 0.6 $ng\,m^{-2}\,h^{-1}$ in the summer and winter month) is lower than the value from soil under the canopy (4.3 and 2.7 $ng\,m^{-2}\,h^{-1}$) because of the landuse classification. The bare lands in the domain include sparsely vegetated land, bare ground tundra and snow/ice land. The flux contribution from such landuse types is largely from the south. The simulated flux from soil under canopy is comparable to those reported at background sites, −0.1 ~ 7 $ng\,m^{-2}\,h^{-1}$ (Carpi and Lindberg, 1998; Ericksen et al., 2006; Kuiken et al., 2008a, b).

The simulated Hg^0 flux from soil under canopy is controlled by the degree of vegetation coverage (LAI), air temperature, friction velocity, air Hg concentration and solar irradiation. In the summer month, the flux in eastern US is lower due to heavy vegetation coverage that increases the in-canopy aerodynamic resistance (R_{ac}) (Zhang et al., 2002a). Higher flux occurs in the Central and Western US because of the smaller LAI

ACPD
13, 32229–32267, 2013

and higher air temperature (Figs. 2c and S8). In the winter month, the higher air temperature and longer sunlit hours cause the higher flux in the south (Figs. 3c and S8). Among the environmental parameters, LAI has the greatest influence on the estimated flux (r = 0.45). The spatially average soil flux for the entire domain shows a typical diurnal variation caused by air temperature and solar irradiance (Gabriel et al., 2006). The detailed impact of the model variables is discussed in the sensitivity analysis.

3.1.3 Air–foliage exchange

Vegetation represents a net sink of Hg^0 in the base-case simulations. The mean simulated air-foliar exchange is −2.2 and $-0.7\,ng\,m^{-2}\,h^{-1}$ in the summer and winter month (Figs. 2d and 3d). The magnitude is similar to those measured in August by Ericksen et al. (2003) (a mean flux of $-3.3\,ng\,m^{-2}\,h^{-1}$) and Millhollen et al. (2006) ($-4.1 \sim -0.3\,ng\,m^{-2}\,h^{-1}$). In summer, the greatest vegetative uptake of Hg^0 occurs in the northeast US because of the dense vegetation coverage. In winter, the uptake becomes much weaker due to the reduced LAI, particularly in the north (Smith-Downey et al., 2010). The simulated deposition flux is highly correlated with LAI (r = 0.71 and 0.88 in winter and summer); while the correlations with friction velocity, GEM, air temperature and solar radiation are comparatively weaker. The diurnal variation for foliar flux is shown in Fig. 4c. Higher deposition occurs during daytime due to the higher air temperature and solar irradiance (Rutter et al., 2011). The overall diurnal variation in the model domain exhibits the feature of air–foliage exchange (Fig. 4d).

The simulated flux from soil under canopy and foliar surfaces is highly dependent on the resistance terms. Presently the values of cuticular (R_c), stomatal (R_g) and soil (R_s) resistances of Hg are not well understood (Holmes et al., 2011) and have been estimated by relating to the measured resistance of O_3, SO_2 and H_2O (Bash, 2010; Scholtz et al., 2003; Zhang et al., 2003). There has been experimental efforts to determine R_c and R_s based on Fick's Law by introducing isotopic Hg tracer to plants grown in an environmentally controlled chamber (Rutter et al., 2011). The resistances were found to depend on temperature, solar irradiance and Hg species with reported R_c

ACPD
13, 32229–32267, 2013

and R_s ranging from 150 to 50 000 $m\,s^{-1}$ at 0–35 °C and 0–170 $W\,m^{-2}$ (Millhollen et al., 2006; Rutter et al., 2011). The simulated flux in the base case applied similar resistance values in the model. However, the lack of deterministic relationships between the resistance terms and environmental parameters still represents a challenge for model estimation and there is a need to better quantify the resistance for Hg^0.

3.2 Sensitivities analysis

3.2.1 Sensitivity on exchanges over water bodies

Figure 5 shows the change of air–water flux due to the change of model variables from the low to the high experimental level (Table 2). Individually, wind speed is the most significant parameter ($p = 0.003$) followed by DGM ($p = 0.004$) and surface temperature ($p = 0.059$). On average, increasing wind speed from 0.001 to 20 $m\,s^{-1}$ enhanced the flux by 7.6 $ng\,m^{-2}\,h^{-1}$ ($p = 0.003$); increasing the DGM from 15 to 240 $ng\,m^{-3}$ increases the flux by 7.0 $ng\,m^{-2}\,h^{-1}$ ($p = 0.004$). A higher air Hg^0 concentration slightly decreases the evasion flux. There is a significant synergistic effect caused by wind speed and DGM concentration ($p = 0.004$). Increasing both variables simultaneously from the low to high level (Table 2) causes an additional 48 % increase of the evasion flux. The wind speed and surface temperature also have a synergistic effect, although not as significant ($p = 0.059$), followed by the effect enhanced by DGM concentration and surface temperature ($p = 0.076$). The effects of higher DGM concentration and air Hg^0 concentration offset each other, leading to a nearly zero effect on flux ($p = 1.000$).

In the base case, a uniform DGM concentration was assumed. The spatially constant DGM level represents a significant uncertainty since other environmental parameters such temperature, wind speed can be estimated reliably through meteorological simulations at a high spatial resolution. The mechanism leading to DGM formation in surface water is complex and not fully understood (Qureshi et al., 2010). It has been suggested that dissolved organic matter (Amyot et al., 1997; Amyot et al., 1994), hydroxyl radicals (Zhang and Lindberg, 2001) and oxyhalide radicals (e.g. OCl^-, OBr^-)

ACPD
13, 32229–32267, 2013

(Lalonde et al., 2001) can participate in the sunlight-induced processes that produce DGM. Data on measured DGM concentration over vast water bodies are not readily available because of a limited number of cruise campaigns (Andersson et al., 2011; Mason et al., 1998, 2001b). More knowledge on the temporal and spatial distribution of DGM concentration in surface water can greatly reduce the model uncertainty. Experimental investigation to better understand the chemical pathways leading to DGM formation will also help constrain the model estimate.

3.2.2 Sensitivity on exchange over bare lands

Figure 6 illustrates the model response to the model variables at the two experimental levels in Table 3. Soil Hg content, friction velocity, air temperature and the scaling factor β_{Hg^0} (Eq. 7) have a positive effect on the simulated Hg flux while the soil organic content has a negative effect. On average, increasing soil Hg content from 50 to 1000 $ng\,g^{-1}$ soil enhances the flux by 55.3 $ng\,m^{-2}\,h^{-1}$ ($p = 0.013$), while increasing friction velocity from 0.0001 to 1 $m\,s^{-1}$ increases the flux by 54.8 $ng\,m^{-2}\,h^{-1}$ ($p = 0.014$). On the other hand, increasing the soil organic content from 0.6 to 10 % reduce the flux by 54.2 $ng\,m^{-2}\,h^{-1}$ ($p = 0.015$). There are several notable interactions among the model variables. First, the positive effects of soil Hg content and friction velocity can be completely offset by soil organic content (Fig. 6). An increase in soil organic content substantially decreases the soil Hg compensation point (Eq. 6), suggesting the significant role of soil organic matter in retaining Hg from evading ($p = 0.025$). There is a strong synergistic effect between friction velocity and soil Hg content ($p = 0.022$), leading to an additional 46 % increase compared to the sum of the two individual effects (Fig. 6). Quasi-laminar sublayer resistance (R_b) and aerodynamic resistance (R_a) both decrease with increasing friction velocity. Coupled with the increased soil Hg compensation point at higher soil Hg content (Eq. 6), the flux is greatly enhanced (Fig. 6). Overall, that friction velocity, soil Hg and organic content are the most influential parameters for Hg exchanges over

ACPD
13, 32229–32267, 2013

bare lands. Other pre-screened parameters including temperature, scaling factor of Hg reactivity (β_{Hg} in Eq. 7) and other interaction terms have a less significant impact.

3.2.3 Sensitivity on exchange over canopy

Figure 7 illustrates the sensitivity of simulated Hg flux over canopy to the model variables at the two experimental levels in Table 4. For comparison, the sensitivity results for air–soil exchange under canopy are also shown. It is clear that the overall air-canopy exchange is dominated by the air–soil exchange under canopy at the two experimental levels. This resembles the Hg^0 emission characteristics observed in a gas exchange system, which showed that the evasion from soils is much greater than the emission from the plants grown in the chamber (Frescholtz and Gustin, 2004; Frescholtz et al., 2003). After the factor pre-screening step (Figs. S2–S7 in the Supplement), the simulated flux is particularly sensitive to the change of five parameters. Friction velocity (positive effect, $p = 0.020$), soil Hg content (positive effect, $p = 0.028$) and soil organic content (negative effect, $p = 0.030$) are the most significant model parameters (Fig. 7). These effects are similar to the sensitivity results of air–soil exchange over bare lands (Figs. 6 and 7), but slightly weaker based on the p values because of the "shielding" of vegetation coverage that modifies the values of the resistance terms (R_b and R_{ac}) (Zhang et al., 2002a). Highly moist soil (soil moisture content > 20 %, Table 4) has a negative effect because it effectively increases soil diffusion resistance (R_g) (Zhang et al., 2003), although the effect is less significant ($p = 0.289$). Air temperature also has a positive effect as anticipated ($p = 0.180$).

The synergistic effect caused by friction velocity and soil Hg content is significant for the air-canopy exchange ($p = 0.028$, Fig. 7), enhancing the evasion flux by 47 % (77.8 ng m^{-2} h^{-1}). Both soil organic content and highly moist soil condition can offset the positive effects caused by higher friction velocity, soil Hg content and air temperature at different degrees (Fig. 7), with the soil organic content being more influential. Higher soil organic content at high soil moisture (> 20 %) yields a weak positive effect ($p = 0.340$) since the combined negative effect of the two parameters is less nega-

ACPD
13, 32229–32267, 2013

tive than the sum of the two individual effects. Overall, these characteristics resemble the air–soil exchange because the air-canopy exchange is dominated by the air–soil exchange under canopy.

Atmospheric mercury can deposit on the surface of cuticle or be accumulated in leaves through stomatal uptake (Fig. 1). For cuticular exchange, air temperature has a significant positive effect (Fig. 8). Since air-cuticle exchange is mainly deposition (negative flux), this means that a higher air temperature leads to smaller deposition or greater evasion ($p < 0.001$). Friction velocity has a strong negative effect (i.e., higher deposition at higher friction velocity, $p < 0.001$) on the simulated flux. Higher soil organic content ($p = 0.009$) and highly moist (> 20 %) soil ($p = 0.194$) increase the simulated flux (i.e., weaken the deposition) by decreasing the canopy compensation point (χ_c in Eq. 8). Under the circumstance, Hg deposits preferentially to soil and therefore a reduced deposition on cuticle. Higher soil Hg content decreases the flux ($p = 0.008$) by increasing the overall compensation point (χ_{cnp} in Eq. 8), suggesting greater deposition on cuticle at higher soil Hg content. For stomatal exchange, the trend of single factor effect is the same as that of cuticular exchange.

Several notable interaction effects are observed for foliar exchanges. For cuticle exchange, the deposition is reversed from deposition to evasion at the high air temperature level, leading to the overall positive interaction effect for air temperature and friction velocity (Fig. 8, $p < 0.001$). The positive effect of soil organic content significantly offsets the negative effect of friction velocity ($p = 0.010$) and soil Hg content ($p = 0.016$). For stomatal exchange, the only significant interaction effect is between soil organic and Hg content, which is more dominated by soil organic content. Overall, the foliar exchange is primarily controlled by air temperature and friction velocity because the resistance terms can be affected by the two variables. This is in contrast to the evapotranspiration approach where soil Hg content plays a predominant role in the simulated Hg^0 evasion flux (Bash et al., 2004; Gbor et al., 2006).

In this analysis, the effect of solar irradiance is *not* as significant as the selected parameters under the resistance model scheme and has been ruled out during the

ACPD
13, 32229–32267, 2013

pre-screening for the model variables (Sect. 2.4 and Figs. S2–S6). In the model, solar irradiation can influence the flux in three ways: (1) through modifying the rate constant of Hg(II) reduction in soils and foliage (Eqs. 6, 10 and 16), (2) through forcing the change of aerodynamic resistance (R_a and R_{ac}), and (3) through forcing the change of cuticular and stomatal resistance terms (R_c and R_{st}). For air–soil exchange, the effect of solar irradiance on the reduction rate constant is the most sensitive process (Eqs. 6 and 10). The photoreduction of Hg(II) in soils has been suggested to be responsible for the increased soil flux observed under sunlit condition (Gustin et al., 2002). There have been kinetic studies showing that increasing UV-A intensity by 75 % approximately doubles the photoreduction rate in the aqueous phase (Qureshi et al., 2010). However, the effect of lights on the kinetics of Hg(II) reduction in soils is poorly understood. In this modeling, the photoreduction rate constant was set to a mean value (Eq. 6). This limits a full examination of the true impact of solar irradiation on the simulated Hg flux. Results from experimental studies on Hg(II) photoreduction rates will help reduce this model uncertainty. For foliar exchange, solar irradiation has a weak positive effect on the flux (i.e., slightly weakens deposition, Fig. S4), but has a significant positive effect on the stomatal exchange (p = 0.004, Fig. S5).

4 Conclusions

An updated model for estimating the bidirectional air–surface exchange of Hg is presented based on the current understanding of surface resistance schemes. From the base-case results, water and soil surfaces are net sources and vegetation is a net sink of Hg^0. Each natural surface exhibits a different diurnal and seasonal variation. Sensitivity analysis of model variables using a 2-level factorial design of experiments shows that atmospheric shear flows (surface wind over water and friction velocity of terrestrial surfaces), dissolved gaseous mercury (DGM) concentration, soil organic and Hg content, and air temperature are the most influential factors controlling the magnitude of the atmosphere-biosphere exchange of Hg^0. However, the positive effect of friction

ACPD
13, 32229–32267, 2013

velocity and soil Hg content on the evasion flux from soil and canopy can be greatly offset by the negative effect of soil organic content. Significant synergistic effects are identified between surface wind and DGM level for water surface, and between soil Hg content and friction velocity for soil surface, leading to ~ 50 % enhanced flux in the combined effect compared to the sum of their individual effects. The air–foliar exchange is mainly controlled by surface resistance terms controlled by environmental parameters such as solar irradiation and air temperature.

The uncertainty in this modeling assessment is primarily from the lack of knowledge in (1) the spatial distribution of organic and Hg content in soil and DGM concentration in water, (2) the reduction mechanism and kinetics of Hg(II) in soil and water, and (3) the values of resistance terms over different natural surfaces. More research in providing geospatial distribution of Hg in water and soil will greatly improve the model estimate. Further elucidation on the interaction of Hg and organic carbon in top soil and surface water as well as quantification of the surface resistance terms specific to Hg species will also help improve the model scheme. Recent field and experimental investigations have suggested that organic carbon in soil potentially shapes the distribution of Hg in forest at continental scales (Obrist et al., 2011) and that the long-term Hg evasion from soil is highly related to the Hg and organic carbon interactions (Smith-Downey et al., 2010). Given the predominance of soil organic content in reducing soil Hg evasion flux using the mechanistic approach in this study, soil organic content is likely the controlling factor determining the intensity of air–soil Hg^0 exchange.

Supplementary material related to this article is available online at http://www.atmos-chem-phys-discuss.net/13/32229/2013/acpd-13-32229-2013-supplement.pdf.

Acknowledgements. This work was funded by National "973" Program of China (2013CB430003), National Institute of Food and Agriculture, US Department of Agriculture (2009-38899-20017), and State Key Laboratory of Environmental Geochemistry, IGCAS. The

ACPD
13, 32229–32267, 2013

funding support is gratefully acknowledged. We thank Pruek Pongprueksa for providing Hg concentration/deposition data for this work and Pattarap?rn Singhasuk for creating the visualization in Fig. 1.

References

Akkarappuram, A. F. and Raman, S.: A comparison of surface friction velocities estimated by dissipation and iterative bulk aerodynamic methods during gale, Geophys. Res. Lett., 15, 401–404, 1988.

Amyot, M., Mierle, G., Lean, D. R. S., and Mcqueen, D. J.: Sunlight-induced formation of dissolved gaseous mercury in lake waters. Environ. Sci. Technol., 28, 2366–2371, 1994.

Amyot, M., Gill, G. A., and Morel, F. M. M.: Production and loss of dissolved gaseous mercury in coastal seawater, Environ. Sci. Technol., 31, 3606–3611, 1997.

Andersson, M. E., Gardfeldt, K., Wangberg, I., and Stromberg, D.: Determination of Henry's law constant for elemental mercury, Chemosphere, 73, 587–592, 2008.

Andersson, M. E., Sommar, J., Gardfeldt, K., and Jutterstrom, S.: Air–sea exchange of volatile mercury in the North Atlantic Ocean. Mar. Chem., 125, 1–7, 2011.

Bash, J. O.: Description and initial simulation of a dynamic bidirectional air–surface exchange model for mercury in Community Multiscale Air Quality (CMAQ) model, J. Geophys. Res.-Atmos., 115, D06305, doi:10.1029/2009jd012834, 2010.

Bash, J. O., Miller, D. R., Meyer, T. H., and Bresnahan, P. A.: Northeast United States and southeast Canada natural mercury emissions estimated with a surface emission model, Atmos. Environ., 38, 5683–5692, 2004.

Bash, J. O., Bresnahan, P., and Miller, D. R.: Dynamic surface interface exchanges of mercury: a review and compartmentalized modeling framework, J. Appl. Meteorol. Clim., 46, 1606–1618, 2007.

Calhoun, F. G., Smeck, N. E., Slater, B. L., Bigham, J. M., and Hall, G. F.: Predicting bulk density of Ohio soils from morphology, genetic principles, and laboratory characterization data, Soil Sci. Soc. Am. J., 65, 811–819, 2001.

Capiomont, A., Piazzi, L., and Pergent, G.: Seasonal variations of total mercury in foliar tissues of Posidonia oceanica, J. Mar. Biol. Assoc. UK, 80, 1119–1123, 2000.

ACPD
13, 32229–32267, 2013

Carpi, A. and Lindberg, S. E.: Application of a Teflon (TM) dynamic flux chamber for quantifying soil mercury flux: tests and results over background soil, Atmos. Environ., 32, 873–882, 1998.

Ericksen, J. A., Gustin, M. S., Schorran, D. E., Johnson, D. W., Lindberg, S. E., and Coleman, J. S.: Accumulation of atmospheric mercury in forest foliage, Atmos. Environ., 37, 1613–1622, 2003.

Ericksen, J. A., Gustin, M. S., Xin, M., Weisberg, P. J., and Fernandez, G. C. J.: Air–soil exchange of mercury from background soils in the United States, Sci. Total. Environ., 366, 851–863, 2006.

Fay, L. and Gustin, M.: Assessing the influence of different atmospheric and soil mercury concentrations on foliar mercury concentrations in a controlled environment, Water Air Soil Poll., 181, 373–384, 2007.

Frescholtz, T. F. and Gustin, M. S.: Soil and foliar mercury emission as a function of soil concentration, Water Air Soil Poll., 155, 223–237, 2004.

Frescholtz, T. F., Gustin, M. S., Schorran, D. E., and Fernandez, G. C. J.: Assessing the source of mercury in foliar tissue of quaking aspen, Environ. Toxicol. Chem., 22, 2114–2119, 2003.

Friedli, H. R., Arellano, A. F., Cinnirella, S., and Pirrone, N.: Initial estimates of mercury emissions to the atmosphere from global biomass burning, Environ. Sci. Technol., 43, 3507–3513, 2009.

Gabriel, M. C., Williamson, D. G., Zhang, H., Brooks, S., and Lindberg, S.: Diurnal and seasonal trends in total gaseous mercury flux from three urban ground surfaces, Atmos. Environ., 40, 4269–4284, 2006.

Gbor, P. K., Wen, D. Y., Meng, F., Yang, F. Q., Zhang, B. N., and Sloan, J. J.: Improved model for mercury emission, transport and deposition, Atmos. Environ., 40, 973–983, 2006.

Gower, S. T., Kucharik, C. J., and Norman, J. M.: Direct and indirect estimation of leaf area index, f(APAR), and net primary production of terrestrial ecosystems, Remote Sens. Environ., 70, 29–51, 1999.

Graydon, J. A., St Louis, V. L., Hintelmann, H., Lindberg, S. E., Sandilands, K. A., Rudd, J. W. M., Kelly, C. A., Tate, M. T., Krabbenhoft, D. P., and Lehnherr, I.: Investigation of uptake and retention of atmospheric Hg(II) by boreal forest plants using stable Hg isotopes. Environ. Sci. Technol., 43, 4960–4966, 2009.

Guo, Y. Y., Amundson, R., Gong, P., and Yu, Q.: Quantity and spatial variability of soil carbon in the conterminous United States, Soil Sci. Soc. Am. J., 70, 590–600, 2006.

ACPD
13, 32229–32267, 2013

Gustin, M. S., Biester, H., and Kim, C. S.: Investigation of the light-enhanced emission of mercury from naturally enriched substrates, Atmos. Environ., 36, 3241–3254, 2002.
Gustin, M. S., Lindberg, S. E., and Weisberg, P. J.: An update on the natural sources and sinks of atmospheric mercury, Appl. Geochem., 23, 482–493, 2008.
Hartman, J. S., Weisberg, P. J., Pillai, R., Ericksen, J. A., Kuiken, T., Lindberg, S. E., Zhang, H., Rytuba, J. J., and Gustin, M. S.: Application of a rule-based model to estimate mercury exchange for three background biomes in the continental United States, Environ. Sci. Technol., 43, 4989–4994, 2009.
Holmes, H. A., Pardyjak, E. R., Perry, K. D., and Abbott, M. L.: Gaseous dry deposition of atmospheric mercury: a comparison of two surface resistance models for deposition to semiarid vegetation, J. Geophys. Res.-Atmos., 116, D14306, doi:10.1029/2010JD015182, 2011.
Jones, R. J. A., Hiederer, R., Rusco, E., Loveland, P. J., and Montanarella, L.: The map of organic carbon in topsoils in Europe, Version 1.2, September 2003: Explanation of Special Publication Ispra 2004 No.72 (S.P.I.04.72). European Soil Bureau Research Report No.17, EUR 21209 EN, 26 pp. and 1 map in ISO B1 format. Office for Official Publications of the European Communities, Luxembourg, 2004.
Kuiken, T., Gustin, M., Zhang, H., Lindberg, S., and Sedinger, B.: Mercury emission from terrestrial background surfaces in the eastern USA, II: air/surface exchange of mercury within forests from South Carolina to New England, Appl. Geochem., 23, 356–368, 2008a.
Kuiken, T., Zhang, H., Gustin, M., and Lindberg, S.: Mercury emission from terrestrial background surfaces in the eastern USA, Part I: air/surface exchange of mercury within a southeastern deciduous forest (Tennessee) over one year, Appl. Geochem., 23, 344–355, 2008b.
Kwun, J. H. and You, S. H.: Numerical study of sea winds simulated by the high-resolution Weather Research and Forecasting (WRF) Model, Asia-Pacific J. Atmos. Sci., 45, 523–554, 2009.
Lalonde, J. D., Amyot, M., Kraepiel, A. M. L., and Morel, F. M. M.: Photooxidation of Hg(0) in artificial and natural waters, Environ. Sci. Technol., 35, 1367–1372, 2001.
Lin, C. J., Lindberg, S. E., Ho, T. C., and Jang, C.: Development of a processor in BEIS3 for estimating vegetative mercury emission in the continental United States, Atmos. Environ., 39, 7529–7540, 2005.
Lin, C. J., Pongprueksa, P., Lindberg, S. E., Pehkonen, S. O., Byun, D., and Jang, C.: Scientific uncertainties in atmospheric mercury models I: model science evaluation, Atmos. Environ., 40, 2911–2928, 2006.

ACPD
13, 32229–32267, 2013

Lin, X. and Tao, Y.: A numerical modelling study on regional mercury budget for eastern North America, Atmos. Chem. Phys., 3, 535–548, doi:10.5194/acp-3-535-2003, 2003.
Lindberg, S., Bullock, R., Ebinghaus, R., Engstrom, D., Feng, X., Fitzgerald, W., Pirrone, N., Prestbo, E., and Seigneur, C.: A synthesis of progress and uncertainties in attributing the sources of mercury in deposition, Ambio, 36, 19–32, 2007.
Marsik, F. J., Keeler, G. J., and Landis, M. S.: The dry-deposition of speciated mercury to the Florida Everglades: measurements and modeling, Atmos. Environ., 41, 136–149, 2007.
Mason, R. P. and Sheu, G. R.: Role of the ocean in the global mercury cycle, Global Biogeochem. Cy., 4, 1093, doi:10.1029/2001GB001440, 2002.
Mason, R. P., Rolfhus, K. R., and Fitzgerald, W. F.: Mercury in the North Atlantic, Mar. Chem., 61, 37–53, 1998.
Mason, R. P., Lawson, N. M., and Sheu, G. R.: Mercury in the Atlantic Ocean: factors controlling air–sea exchange of mercury and its distribution in the upper waters, Deep-Sea Res. II, 48, 2829–2853, 2001a.
Mason, R. P., Sheu, G. R., and Lawson, N. M.: Redox chemistry of mercury at the air–water interface and its role in the global cycling of mercury, Abstr. Pap. Am. Chem. S., 222, U429–U429, 2001b.
Millhollen, A. G., Gustin, M. S., and Obrist, D.: Foliar mercury accumulation and exchange for three tree species, Environ. Sci. Technol., 40, 6001–6006, 2006.
Morel, F. M. M., Kraepiel, A. M. L., and Amyot, M.: The chemical cycle and bioaccumulation of mercury, Annu. Rev. Ecol. Syst., 29, 543–566, 1998.
Myers, R. H., Montgomery, D. C., and Anderson-Cook, C. M.: Response Surface Methodology: Process and Product Optimization Using Designed Experiments, 3 Edn, John Wiley & Sons Inc., New York, 2009.
Obrist, D., Johnson, D. W., Lindberg, S. E., Luo, Y., Hararuk, O., Bracho, R., Battles, J. J., Dail, D. B., Edmonds, R. L., Monson, R. K., Ollinger, S. V., Pallardy, S. G., Pregitzer, K. S., and Todd, D. E.: Mercury distribution across 14 US forests, Part I: spatial patterns of concentrations in biomass, litter, and soils, Environ. Sci. Technol., 45, 3974–3981, 2011.
Pacyna, J. M., Pacyna, E. G., Steenhuisen, F., and Wilson, S.: Mapping 1995 global anthropogenic emissions of mercury, Atmos. Environ., 37, S109-S117, 2003.
Pacyna, E. G., Pacyna, J. M., Steenhuisen, F., and Wilson, S.: Global anthropogenic mercury emission inventory for 2000, Atmos. Environ., 40, 4048–4063, 2006.

ACPD
13, 32229–32267, 2013

Pirrone, N., Cinnirella, S., Feng, X., Finkelman, R. B., Friedli, H. R., Leaner, J., Mason, R., Mukherjee, A. B., Stracher, G. B., Streets, D. G., and Telmer, K.: Global mercury emissions to the atmosphere from anthropogenic and natural sources, Atmos. Chem. Phys., 10, 5951–5964, doi:10.5194/acp-10-5951-2010, 2010.

Poissant, L., Amyot, M., Pilote, M., and Lean, D.: Mercury water-air exchange over the upper St. Lawrence River and Lake Ontario, Environ. Sci. Technol., 34, 3069–3078, 2000.

Poissant, L., Pilote, M., Yumvihoze, E., and Lean, D.: Mercury concentrations and foliage/atmosphere fluxes in a maple forest ecosystem in Quebec, Canada, J. Geophys. Res.-Atmos., 113, D10307, doi:10.1029/2007jd009510, 2008.

Qureshi, A., O'Driscoll, N. J., MacLeod, M., Neuhold, Y. M., and Hungerbuhler, K.: Photoreactions of mercury in surface ocean water: gross reaction kinetics and possible pathways, Environ. Sci. Technol., 44, 644–649, 2010.

Rutter, A. P., Schauer, J. J., Shafer, M. M., Creswell, J., Olson, M. R., Clary, A., Robinson, M., Parman, A. M., and Katzman, T. L.: Climate sensitivity of gaseous elemental mercury dry deposition to plants: impacts of temperature, light intensity, and plant species, Environ. Sci. Technol., 45, G03008, doi:10.1029/2009JG001124, 2011.

Scholtz, M. T., Van Heyst, B. J., and Schroeder, W.: Modelling of mercury emissions from background soils, Sci. Total. Environ., 304, 185–207, 2003.

Shetty, S. K., Lin, C. J., Streets, D. G., and Jang, C.: Model estimate of mercury emission from natural sources in East Asia, Atmos. Environ., 42, 8674–8685, 2008.

Smith-Downey, N. V., Sunderland, E. M., and Jacob, D. J.: Anthropogenic impacts on global storage and emissions of mercury from terrestrial soils: insights from a new global model, J. Geophys. Res.-Biogeo., 115, , 2010.

Stamenkovic, J. and Gustin, M. S.: Nonstomatal vs. stomatal uptake of atmospheric mercury, Environ. Sci. Technol., 43, 1367–1372, 2009.

Streets, D. G., Hao, J. M., Wu, Y., Jiang, J. K., Chan, M., Tian, H. Z., and Feng, X. B.: Anthropogenic mercury emissions in China, Atmos. Environ., 39, 7789–7806, 2005.

Streets, D. G., Zhang, Q., and Wu, Y.: Projections of global mercury emissions in 2050, Environ. Sci. Technol., 43, 2983–2988, 2009.

Sutton, M. A., Nemitz, E., Erisman, J. W., Beier, C., Bahl, K. B., Cellier, P., de Vries, W., Cotrufo, F., Skiba, U., Di Marco, C., Jones, S., Laville, P., Soussana, J. F., Loubet, B., Twigg, M., Famulari, D., Whitehead, J., Gallagher, M. W., Neftel, A., Flechard, C. R., Herrmann, B., Calanca, P. L., Schjoerring, J. K., Daemmgen, U., Horvath, L., Tang, Y. S., Em-

ACPD
13, 32229–32267, 2013

mett, B. A., Tietema, A., Penuelas, J., Kesik, M., Brueggemann, N., Pilegaard, K., Vesala, T., Campbell, C. L., Olesen, J. E., Dragosits, U., Theobald, M. R., Levy, P., Mobbs, D. C., Milne, R., Viovy, N., Vuichard, N., Smith, J. U., Smith, P., Bergamaschi, P., Fowler, D., and Reis, S.: Challenges in quantifying biosphere-atmosphere exchange of nitrogen species, Environ. Pollut., 150, 125–139, 2007.

USEPA: User's Guide for Evaluating Subsurface Vapor Instrusion Into Buildings (User's Guide),: US Environmental Protection Agency, Washington, DC, 2004.

Xu, X. H., Yang, X. S., Miller, D. R., Helble, J. J., and Carley, R. J.: Formulation of bi-directional atmosphere-surface exchanges of elemental mercury, Atmos. Environ., 33, 4345–4355, 1999.

Zehner, R. E. and Gustin, M. S.: Estimation of mercury vapor flux from natural substrate in Nevada, Environ. Sci. Technol., 36, 4039–4045, 2002.

Zhang, H. and Lindberg, S. E.: Sunlight and iron(III)-induced photochemical production of dissolved gaseous mercury in freshwater, Environ. Sci. Technol., 35, 928–935, 2001.

Zhang, L., Brook, J. R., and Vet, R.: A revised parameterization for gaseous dry deposition in air-quality models, Atmos. Chem. Phys., 3, 2067–2082, doi:10.5194/acp-3-2067-2003, 2003.

Zhang, L., Wright, L. P., and Blanchard, P.: A review of current knowledge concerning dry deposition of atmospheric mercury, Atmos. Environ., 43, 5853–5864, 2009.

Zhang, L., Blanchard, P., Gay, D. A., Prestbo, E. M., Risch, M. R., Johnson, D., Narayan, J., Zsolway, R., Holsen, T. M., Miller, E. K., Castro, M. S., Graydon, J. A., Louis, V. L. St., and Dalziel, J.: Estimation of speciated and total mercury dry deposition at monitoring locations in eastern and central North America, Atmos. Chem. Phys., 12, 4327–4340, doi:10.5194/acp-12-4327-2012, 2012.

Zhang, L. M., Brook, J. R., and Vet, R.: On ozone dry deposition – with emphasis on non-stomatal uptake and wet canopies, Atmos. Environ., 36, 4787–4799, 2002a.

Zhang, L. M., Moran, M. D., Makar, P. A., Brook, J. R., and Gong, S. L.: Modelling gaseous dry deposition in AURAMS: a unified regional air-quality modelling system, Atmos. Environ., 36, 537–560, 2002b.

Zhang, L. M., Wright, L. P., and Blanchard, P.: A review of current knowledge concerning dry deposition of atmospheric mercury, Atmos. Environ., 43, 5853–5864, 2009b.

Zotarelli, L., Dukes, D. M., and Morgan, K. T.: Interpretation of Soil Moisture Content to Determine Soil Field Capacuty and Avoid Over-Orrigating Sandy Soils Using Soil Moisture Sen-

ACPD
13, 32229–32267, 2013

sors, The Agricultural and Biological Engineering Department, Florida Cooperative Extension Service, Institute of Food and Agricultural Sciences, University of Florida. AE460, 2010.

ACPD
13, 32229–32267, 2013

Table 1. Model variables and units in the base-case simulation.

Term	Description	Value or units
F_w	Flux from water bodies	ng m^{-2} h^{-1}
K_w	Mass transfer coefficient of mercury through water layer	m h^{-1}
C_w	DGM concentration	40 ng m^{-3} water[a]
H_w	Henry's law constant under water conditions	dimensionless
F_{cnp}	The flux over canopy biomes	ng m^{-2} h^{-1}
Δt	Time duration	s
R_a	Aerodynamic resistance	s m^{-1}
R_b	Quasi-laminar sub-layer resistance	s m^{-1}
C_{atm}	Atmospheric Hg concentration	ng m^{-3}
χ_{cnp}	The total compensation point	ng m^{-3}
χ_c	Cuticular interfaces compensation point	ng m^{-3}
χ_s	Stomatal interfaces compensation point	ng m^{-3}
χ_g	Soil interfaces compensation point	ng m^{-3}
R_c	cuticular resistance	s m^{-1}
R_s	stomatal resistance	s m^{-1}
R_g	soil diffusion resistance	s m^{-1}
R_{ac}	in-canopy aerodynamic resistance	s m^{-1}
F_{bls}	the flux from bare land soil	ng m^{-3}
$\left[Hg^0\right]_{sl}$	elemental mercury content bound to organic matter	ng g^{-1} soil
H	Henry's Law constant in soil condition	dimensionless
f_{oc}	fraction of organic carbon in topsoil (0–5 cm)	2 % (dimensionless)[b]
K_{oc}	soil organic carbon to water partitioning coefficient	m^3 water g^{-1} organic carbon
$[Hg(II)]_{sl}$	Hg(II) content in the soil	90 ng g^{-1} soil[c]
$R_{g(SO_2)}$	SO_2 soil diffusion resistance	s m^{-1}
$R_{g(O_3)}$	O_3 soil diffusion resistance	s m^{-1}
α_{Hg^0}	Hg scaling factor basing on SO_2	0 (dimensionless)[d]
β_{Hg^0}	Hg scaling factor basing on O_3	.1 (dimensionless)[e]
LAP	leaf-air partitioning coefficient for Hg between leaves and air	30 000 (dimensionless)[f]

ACPD
13, 32229–32267, 2013

Table 1. Continued.

Term	Description	Value or units
$[Hg^0_c]$	Hg^0 content bound to foliar cuticular surface	$ng\,m^{-3}$ leaf
$\left[Hg^{II+}_c\right]$	newly dry deposited Hg(II) residing on cuticular surfaces	$ng\,m^{-2}$ leaf
$[Hg^{II+}_{c,DD}]$	the total dry deposited Hg(II) loading on cuticular compartment	$ng\,m^{-2}$ leaf
$[Hg^{II+}_w]$	Hg(II) leaf wash concentration	$0.04\,ng\,m^{-2}$ leaf [g]
f_{rxn}	fraction of Hg(II) potentially photo-reduced to Hg	dimensionless
f_{fixed}	fraction of Hg(II) being fixed into tissue	dimensionless
T_l	leaf thickness	0.000152 m[h]
$[Hg^0_s]$	Dissolved elemental mercury in stomatal compartment	$ng\,m^{-3}$ leaf
$[Hg^0_{s,DD}]$	deposited Hg concentration stored inside stomatal compartment	$0.39\,ng\,m^{-2}$ leaf h^{-1}[i]
R_{st}	resistance associating stomata apertures	$s\,m^{-1}$
R_{me}	resistance associating mesophyll reservoir	$s\,m^{-1}$
W_{st}	fraction of stomatal blocking under wet condition	dimensionless

[a]Value for base-case simulation (Xu et al., 1999).
[b]For 0–20 cm topsoil, the bulk density is 1.1–1.3 $g\,cm^{-3}$ and organic carbon content is 3.3 $kg\,m^{-2}$ in the US (Calhoun et al., 2001; Guo et al., 2006), so assuming in the 0–5 cm topsoil foc is 2 %.
[c]Value for base-case simulation (Bash, 2010).
[d]Basing on the negligible solubility (Henry's constant = 0.139 $M\,atm^{-1}$) and chemical inertness (Zhang et al., 2012; Zhang et al., 2009b).
[e]Zhang et al. (2012).
[f]Rutter et al. (2011a).
[g]Value for base-case simulation, (Frescholtz et al., 2003).
[h]Value for base-case simulation (Abrams and Kubiske, 1990).
[i]Value for base-case simulation (Poissant et al., 2008).

ACPD
13, 32229–32267, 2013

Table 2. Examined model variables and the experimental levels of factorial design for air-water exchange.

Term	Description	Low level	High level
T	Sea surface temperature (°C)	-2^{a}	35^{a}
GEM	Air Hg^0 concentration ($ng\,m^3$)	1.0^{b}	2.0^{b}
DGM	Dissolved Hg^0 concentration in surface water($ng\,m^{-3}$)	15^{c}	240^{c}
W	Wind speed at 10 m above water surface ($m\,s^{-1}$)	0.001^{d}	20^{d}

[a] Kwun and You (2009)
[b] According to global background of air Hg^0 at 1.1 ~ 1.7 $ng\,m^3$ (Lindberg et al., 2007).
[c] Morel et al. (1998).
[d] Andersson et al. (2011).

ACPD
13, 32229–32267, 2013

Table 3. Examined model variables and the experimental levels of factorial design for air–soil exchange over sparsely vegetated land, bare ground tundra and snow/ice land.

Term	Description	Low level	High level
T	Air temperature at 2 m (°C)	−2	40
$Q2$	Water vapor mixing ratio (Kg Kg^{-1})	0.0005[a]	0.05[a]
f_{oc}	Fraction of organic carbon in surface soil	0.006[b]	0.1[c]
UST	Friction velocity(m s^{-1})	0.0001[d]	1.0[d]
SM	Soil Hg content (ng g^{-1} soil)	50[e]	1000[e]
GEM	Air Hg^0 concentration (ng m^{-3})	1.0	2.0
SNOWH	Snow depth (m)	0[f]	0.4999 [f]
β_{Hg0}	Scaling factor of reactivity Hg	0.1[g]	0.2[h]
DC	Dew condition	No[i]	Yes[i]
RC	Rain condition	No[j]	Yes[j]
MC	Moist soil condition	No[l]	Yes[l]

[a]Kwun and You (2009).
[b]Suggested default value for modeling of volatilized contaminant to air by USEPA (2004).
[c]Upper limit of the forest soils (Jones et al., 2004).
[d]Akkarappuram and Raman (1988).
[e]Carpi and Lindberg (1998);[6] Has effect on ground and cuticular resistance, (Zhang et al., 2003).
[f]Zhang et al. (2012).
[g]Zhang et al. (2009a).
[h]Air temperature below dew point represents low level and vice versa, has effect on ground and cuticular resistance (Zhang et al., 2003).
[i]Has effect on ground and cuticular resistance terms (Zhang et al., 2003).
[j]Soil moisture > 20 % represents low level and vice versa, the high level suggests highly moist soil (Zotarelli et al., 2010).

ACPD
13, 32229–32267, 2013

Table 4. Examined model variables and the experimental levels of factorial design for air-canopy exchange.

Term	Description	Low level	High level
T	Air temperature at 2 m (°C)	−2	40
f_{oc}	Fraction of organic carbon in surface soil	0.006	0.1
UST	Friction velocity($m\,s^{-1}$)	0.0001	1.0
SM	Soil total Hg content ($ng\,m^{-3}$)	50	1000
β_{Hg0}	Scaling factor of reactivity Hg	0.1	0.2
SNOWH	Snow depth (m)	0	0.4999
LAI	Leaf area index ($m^2\,m^{-2}$)	1.0[a]	5.0[a]
SR	Solar irradiation ($W\,m^{-2}$)	0	1000
Leaf_Hg	Hg concentration in leaf rinse ($ng\,m^{-2}$ leaf)	0.02[b]	2.10[c]
Stomata_Hg	Hg previously deposited to leaf stomata ($ng\,m^{-2}$ leaf)	0.13[d]	0.59[d]
GEM	Air Hg^0 concentration ($ng\,m^{-3}$)	1.0	2.0
LAP	Leaf-air partitioning coefficient (m^3 air m^{-3} leaf)	30 000[e]	6 000 000[e]
DC	Dew condition	No	Yes
RC	Rain condition	No	Yes
MC	Moist soil condition	No	Yes

[a] Gower et al. (1999).
[b] Frescholtz et al. (2003).
[c] Fay and Gustin (2007).
[d] Poissant et al. (2008).
[e] Rutter et al. (2011).

ACPD
13, 32229–32267, 2013

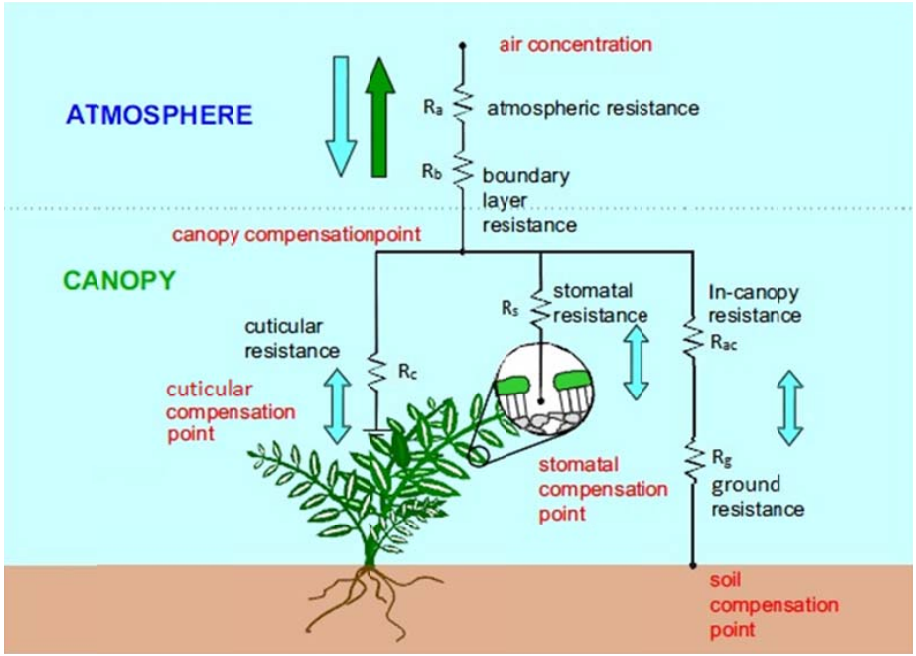

Fig. 1. Resistance scheme implemented in the air–surface exchange model following Sutton et al. (2007) and Zhang et al. (2009a).

ACPD
13, 32229–32267, 2013

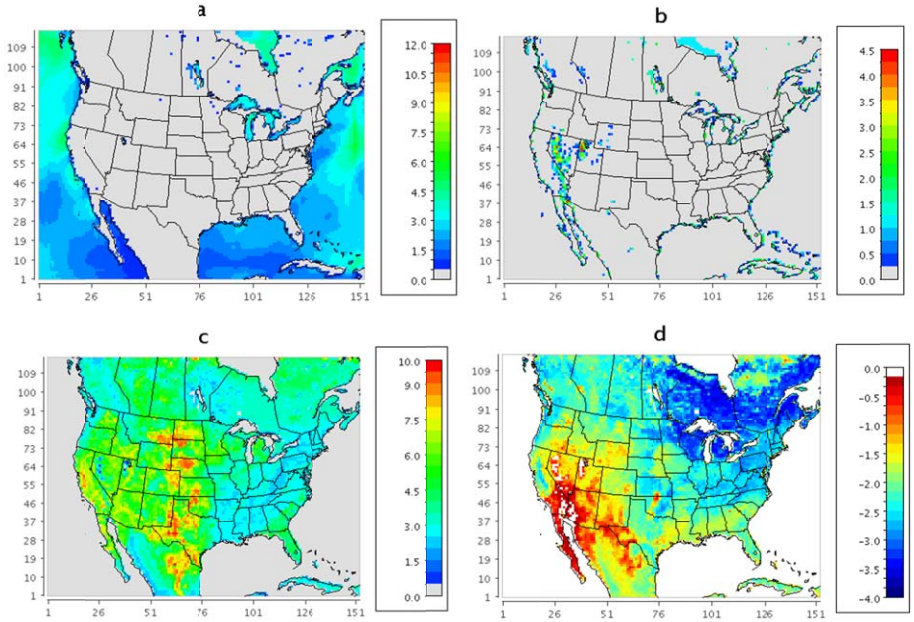

Fig. 2. Monthly mean of the simulated Hg^0 flux (ng $m^{-2} h^{-1}$) in the summer month: **(a)** flux from water body, **(b)** flux from bare lands, **(c)** flux from soil under the canopy, and **(d)** flux from foliage.

ACPD
13, 32229–32267, 2013

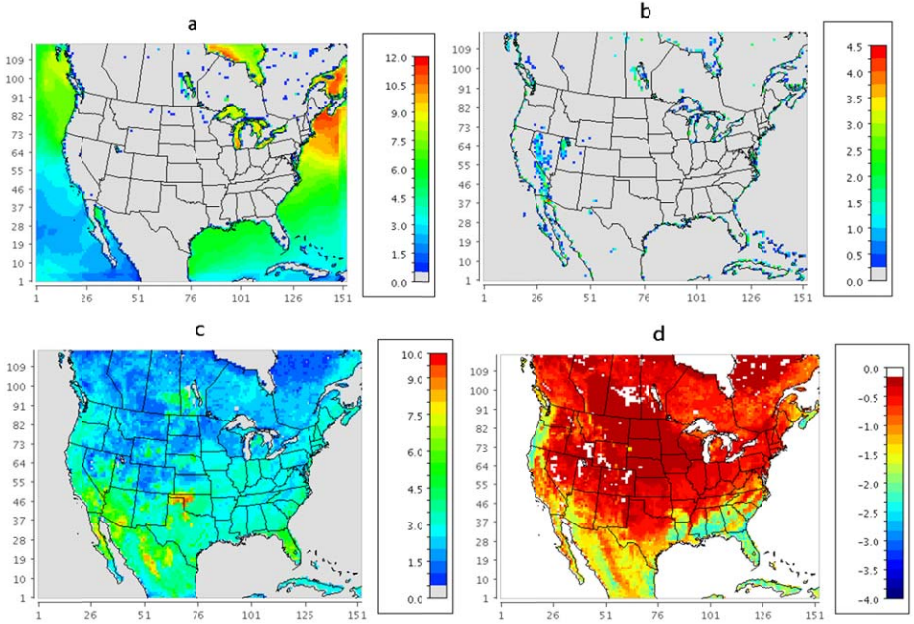

Fig. 3. Monthly mean of the simulated Hg^0 flux ($ng\,m^{-2}\,h^{-1}$) in the winter month: **(a)** flux from water body, **(b)** flux from bare lands, **(c)** flux from soil under the canopy, and **(d)** flux from foliage.

ACPD
13, 32229–32267, 2013

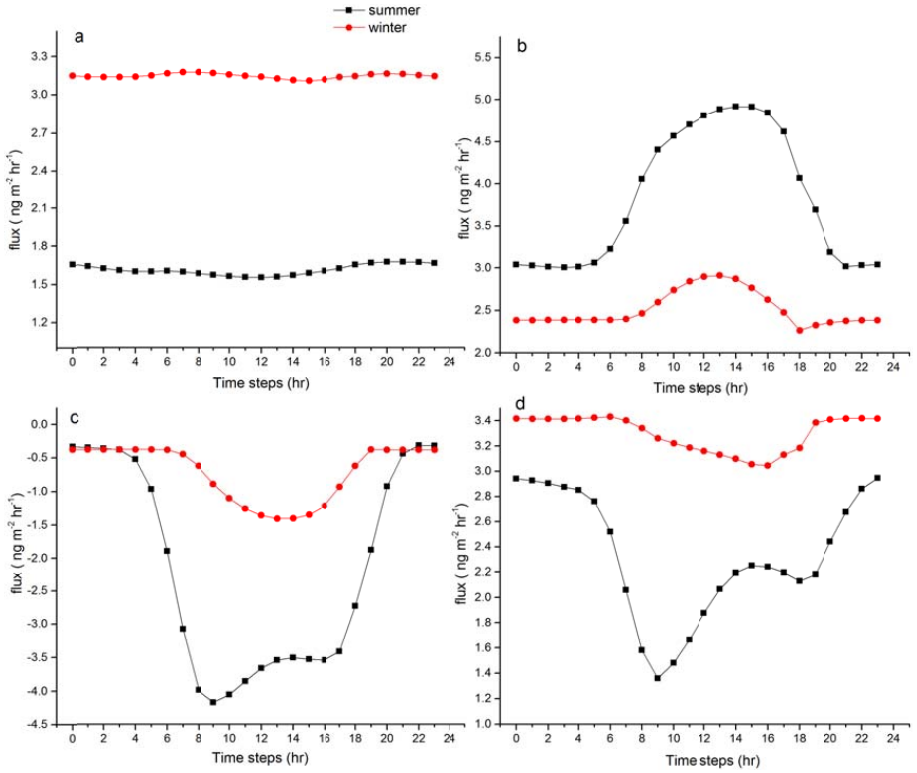

Fig. 4. Diurnal variation of mean simulated Hg^0 for the entire model domain (UTC-7): **(a)** flux from water body, **(b)** total flux from soils (soil under the canopy and bare lands), **(c)** flux from foliage, and **(d)** flux for the total domain.

ACPD
13, 32229–32267, 2013

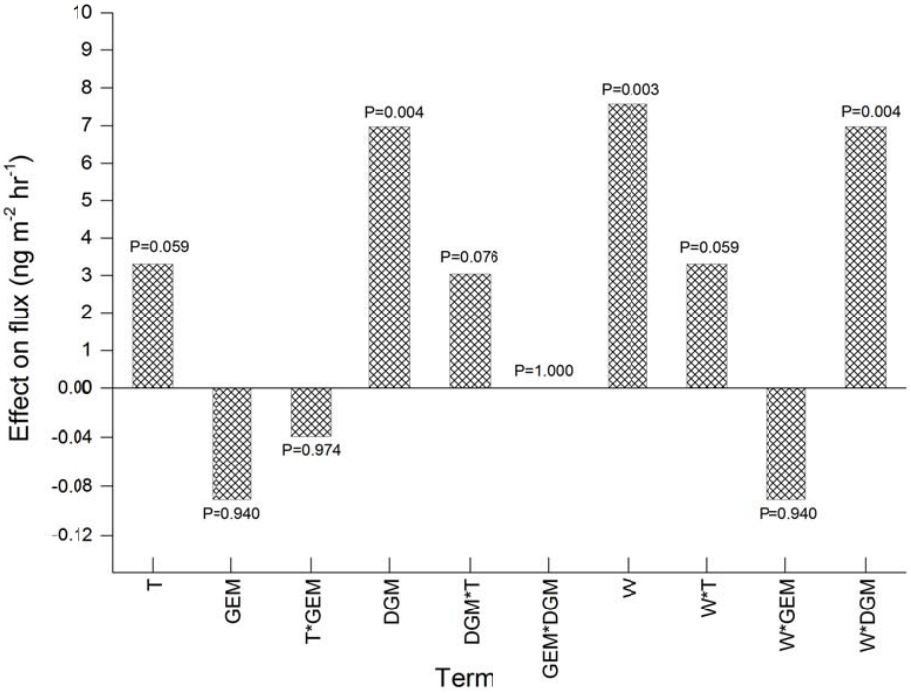

Fig. 5. Sensitivity analysis based on the 2^4 factorial design shown in Table 2 (water body). *T* denotes air temperature at water surface; GEM denotes air Hg concentration; DGM denotes dissolved gaseous Hg concentration in surface water; *W* denotes wind speed. "*" denotes the interaction effects.

ACPD
13, 32229–32267, 2013

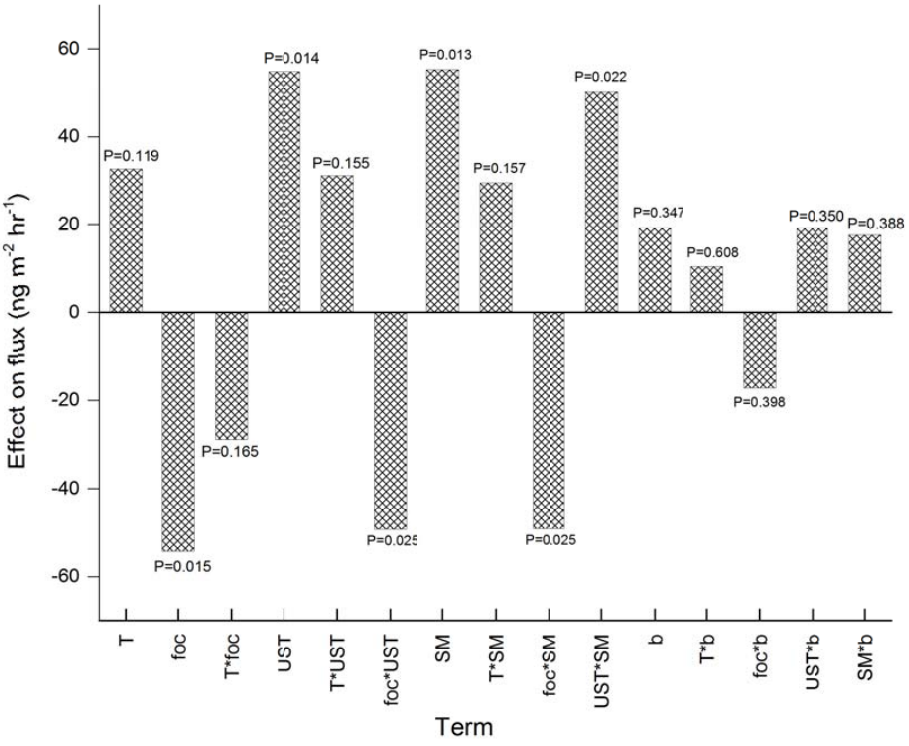

Fig. 6. Sensitivity analysis based on the 2^5 factorial design for bare lands after pre-screening model variables shown in Table 3 to isolate the significant factors. *T* denotes surface air temperature; foc denotes fraction of organic carbon in soil; UST denotes friction velocity; SM denotes soil mercury content; *b* denotes scaling factor for Hg reactivity (β_{Hg0}). "*" denotes interaction effects.

ACPD
13, 32229–32267, 2013

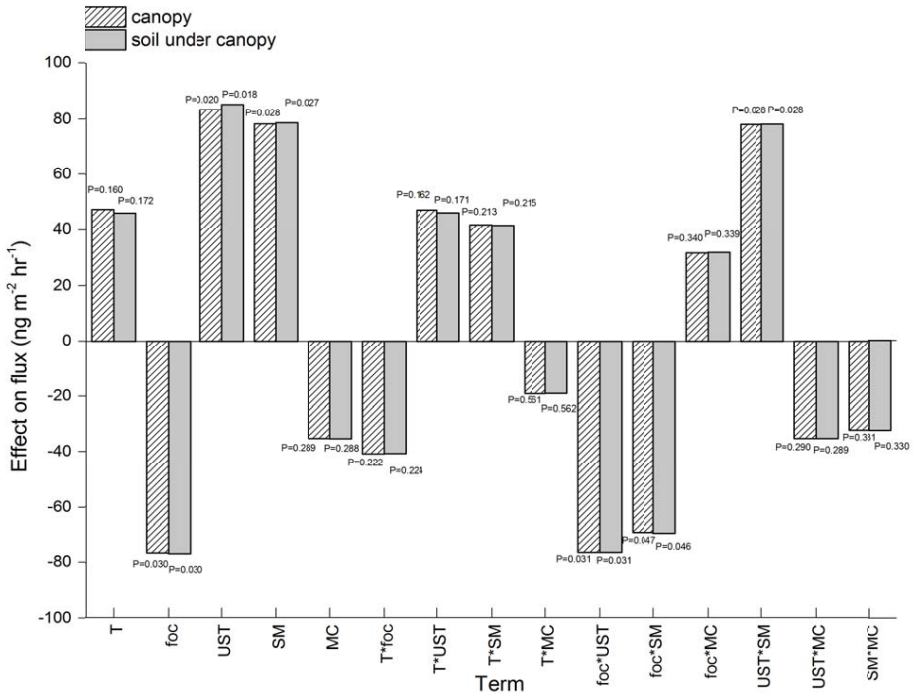

Fig. 7. Sensitivity analysis based on the 2^5 factorial design at canopy level after pre-screening model variables shown in Table 4 to isolate the significant factors. The overall flux at canopy level is dominated by the soil flux under the canopy (the sensitivity of foliar exchange is shown in Fig. 8). *T* denotes surface air temperature; foc denotes fraction of organic carbon in soil; UST denotes friction velocity; SM denotes soil Hg content; MC denotes soil moisture. "*" denotes interaction effects.

ACPD
13, 32229–32267, 2013

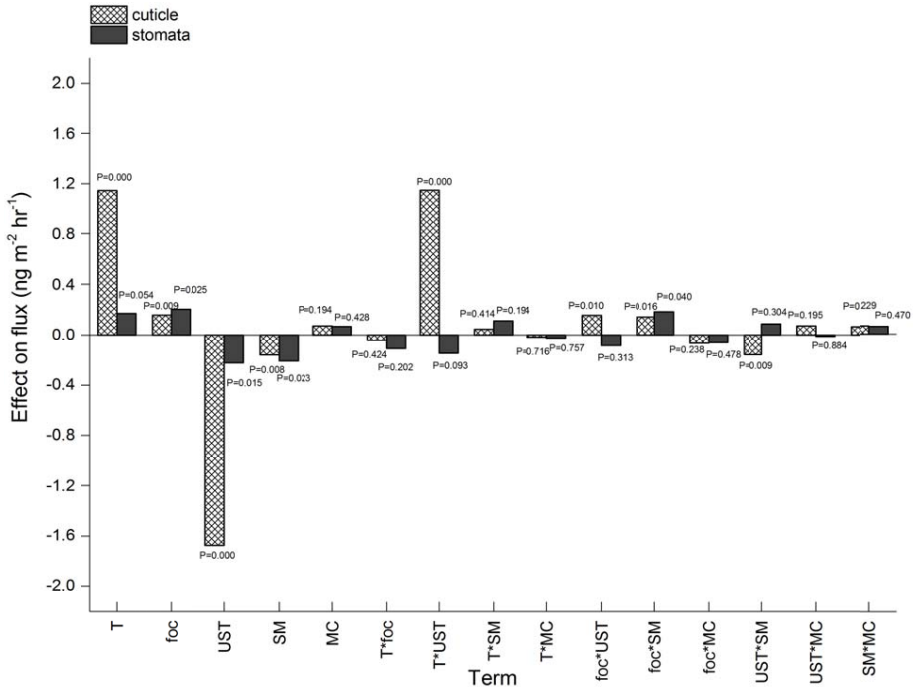

Fig. 8. Sensitivity analysis based on the 2^5 factorial design for foliar exchange after pre-screening model variables shown in Table 4 to isolate the significant factors. *T* denotes surface air temperature; foc denotes fraction of organic carbon in soil; UST denotes friction velocity; SM denotes soil Hg content; MC denotes soil moisture. "*" denotes interaction effects.

ACPD
13, 32229–32267, 2013

Updated bidirectional air-surface exchange model for mercury vapor

X. Wang et al.